43rd AIAA Thermophysics Conference
25 - 28 June 2012, New Orleans, Louisiana

AIAA 2012-2871

Time-dependent Estimation of Mars Science Laboratory Surface Heating from Simulated MEDLI data

Milad Mahzari[1] and Robert D. Braun[2]
Georgia Institute of Technology, Atlanta, GA, 30332

There are substantial uncertainties in the computational models currently used to predict the heating environment and the Thermal Protection System (TPS) material response during Mars entry. Flight data is required to quantify and possibly reduce such uncertainties as well as improve current computational tools. The Mars Science Laboratory (MSL) Entry, Descent and Landing Instrumentation (MEDLI) suite will provide a comprehensive set of flight data which will include subsurface temperature measurements of its PICA heatshield at different locations. Accurate reconstruction of MSL surface heat flux from the flight data is a critical step in reducing these uncertainties. The purpose of this paper is to investigate the time-dependent estimation of MSL surface heating from simulated MEDLI subsurface temperature data using inverse methods in the presence of random and bias measurement and model errors. The surface heat flux is indirectly reconstructed by estimating the discretized surface heat transfer coefficient profile as a function of time. Whole-time domain least-squares methods in conjunction with the Tikhonov regularization technique are applied to this problem. The analysis is performed for the instrument plugs at the lowest and highest heating locations. The performance of the estimation methods and the accuracy of the reconstructed surface conditions are investigated under different types of errors in the measurements such as random noise and thermocouple lag. Furthermore, the effect of material property bias on the estimation of surface conditions is also studied.

Nomenclature

A	=	Surface area
B'	=	Dimensionless surface blowing rate
C_H	=	FIAT heat transfer coefficient = $\rho_e u_e c_h$
Cp	=	Specific heat
h	=	Enthalpy, contact conductance
H1	=	First-order Tikhonov regularization matrix
H_R	=	Total recovery enthalpy
J	=	Sensitivity matrix
$\dot{m}$	=	Surface blowing rate
M	=	Number of measurements
N	=	Number of discretized C_H points
p	=	Pressure
P	=	Vector of estimation parameters
q	=	Heat flux
S	=	Sum of square of errors (objective function)
t	=	Time
T	=	Temperature
T	=	Vector of direct problem outputs (FIAT predictions)
V	=	Volume
Y	=	Vector of measurements
α	=	Surface absorptivity

[1] Graduate Research Assistant, Guggenheim School of Aerospace Engineering, AIAA Student Member.
[2] David and Andrew Lewis Professor of Space Technology, Daniel Guggenheim School of Aerospace Engineering, AIAA Fellow.

ε = Surface emissivity
μ = Regularization parameter
ρ = Density
σ = Stefan-Boltzmann constant

Subscripts
c = Char
cond = Conduction
g = Pyrolysis gas
host = Host material
rad = Radiative
w = Material surface
wire = TC wire properties
∞ = Freestream

Superscripts
BE = Best-estimate
k = Iteration number
Nom = Nominal
T = Transpose of a matrix

I. Introduction

The Thermal Protection System (TPS) is responsible for protecting a spacecraft against entry aeroheating. When spacecraft travel to other planets for surface missions or when they return to Earth upon the completion of their missions, they typically enter a planet's atmosphere at very high velocity to land on the surface. During entry, the interaction between the spacecraft and the planet's atmosphere will generally dissipate more than 90% of the entry system's initial kinetic energy, mostly in the form of heat. The heatshield must keep the aeroshell interior safe from these extreme environments. Since the TPS is critical to mission success, the aeroheating environment and TPS material response have to be modeled accurately. However, there are substantial uncertainties associated with the analytical models that are currently used for predicting aeroheating and TPS response, such as heating augmentation due to turbulence and catalysis, TPS recession prediction and TPS material properties.[1] These uncertainties have a significant effect on the TPS material selection and total heatshield mass, and therefore limit our ability to design more capable and robust Entry, Descent and Landing (EDL) systems.

Flight data can help engineers reduce these uncertainties to improve or validate computational tools. During the past few decades, there have been numerous entry missions that were equipped with instruments to collect aeroheating and TPS performance data, primarily in support of the Apollo program.[2] Lessons have been learned from these efforts, but some of the returned data have either not been critically evaluated or were not sufficient for code validation. A majority of these instrumented missions have occurred in the Earth atmosphere. However, Mars has been and will continue to be a frequent destination in recent space exploration efforts. To date, Viking and Pathfinder have been the only missions equipped with forebody TPS instruments.[3] The need for Martian flight data is further justified since the experimental facilities on Earth are not capable of fully recreating Mars flight conditions. Mars Science Laboratory (MSL), expected to land on Mars in August 2012, is instrumented with aerodynamic and aeroheating sensors. The MSL aeroshell is a 4.5-meter diameter spherically-blunted 70-degree half-angle cone with a triconic afterbody.[4] MSL's heatshield is made of an ablative material called Phenolic Impregnated Carbon Ablator (PICA). A uniform PICA thickness of 1.25 in is used. MSL Entry, Descent, and Landing instrumentation (MEDLI) [5] includes pressure sensors, in-depth thermocouples and isotherm sensors. The MEDLI dataset will provide the first non-Earth entry aeroheating data since the Pathfinder mission and will provide more EDL data than all of the previous Mars missions combined. [5]

The flight data acquired by MEDLI will help answer some of the fundamental questions related to aeroheating and TPS performance while also addressing the uncertainties associated with current tools. A systematic post-flight data analysis strategy is required to maximize the benefits obtained from the MEDLI data. The main goal of this research is to develop a relatively general methodology to analyze MEDLI aeroheating and TPS flight data. The authors previously developed a comprehensive Inverse Parameter Estimation (IPE) methodology for the analysis of

aeroheating and TPS data and applied that methodology to an arc jet test dataset.[6] The previous work focused on the methodology and identification of the material properties and heating parameters are significant uncertainty contributors and which ones can be simultaneously estimated. In reference 6, the surface heating generated in the arc jet was a constant value with no time-dependency. However, in a flight case, the surface heating changes as a function of time. In addition, in flight, the uncertainties in surface heating are more significant than the uncertainties in the material properties. Consequently, an accurate reconstruction of the surface heat flux is a required step to improve the models used to estimate the TPS performance during a Martian entry.

Reconstruction of an entry vehicle's surface heating from TPS subsurface temperature data belongs to the class of Inverse Heat Conduction Problems (IHCP).[7] These problems are mathematically ill-posed and difficult to solve, specifically in the presence of noise or bias error in the data or models. The solution normally involves the minimization of an objective function containing both the predicted and measured temperatures. Different approaches and minimization methods have been developed for the solution of IHCPs and are used in conjunction with regularization techniques[8, 9] to make the problem better conditioned for solution. IHCPs have been studied extensively in the literature; however, the application of these methods to the problem of ablating and pyrolyzing TPS material has not been prevalent.

The objective of this paper is to investigate the time-dependent estimation of MSL surface heating from simulated MEDLI data using inverse methods in preparation for the analysis of the actual flight data. Performing this analysis with simulated data is crucial because we have the benefit of knowing the true solution and it provides us with the opportunity to characterize the performance of the inverse methods in the presence of different measurement and model errors. This work will help identify the limitations of the inverse methods and the level of accuracy that can be achieved for the estimation of surface conditions. In this paper, the heat flux is indirectly reconstructed by estimating discretized surface heat transfer coefficient profile as a function of time. This is done using whole-time domain least-squares methods, specifically the Gauss-Newton method. The Tikhonov first-order technique is used for the regularization of this ill-posed problem. Section II provides an overview of the MEDLI instrumentation suite. Section III describes the methodology and the inverse techniques used in this paper. The process used to investigate IPE methods for this application is also described in this section. Section IV presents the result of the investigation process. Specifically, the effect of different types of measurement errors on the estimation results is explored. Furthermore, the effect of material property bias which comes from an inaccurate knowledge of material properties on the estimation results is investigated.

II. MEDLI

MEDLI consists of seven pressure ports and seven integrated sensor plugs at different locations on the MSL heatshield. The suite consists of three subsystems: MEDLI Integrated Sensor Plug (MISP) temperature/isotherm sensors, Mars Entry Atmospheric Data System (MEADS) pressure sensors, and Sensor Support Electronics (SSE). The sensors are installed into the PICA plugs that are flush-mounted to the flight heatshield. The MISP locations (Figure 1, T labels) cover a broad range of heat flux environments, while the MEADS locations (Figure 1, P labels) are concentrated in the higher pressure and lower heat flux region near the stagnation point and the nose region. The data from the MISP sensors are the focus of this research.

Each MISP plug is 33 mm in diameter with a total depth of 20.3 mm, and contains four type-K U-shaped thermocouples.[5] The thermocouples are approximately at 2.54, 5.08, 10.16, and 15.24 mm from the surface of the plug. The top two thermocouples are intended primarily for heating reconstruction, while the two deeper thermocouples are primarily intended for material property reconstruction. The science measurement range requirement for each thermocouple is 100 to 1300 K with an accuracy of ± 2.2 K or 2.0% below 273 K and ± 1.1 K or 0.4% above 273 K. The top thermocouple is sampled at 8 Hz while the deeper thermocouples are sampled at either 1 or 2 Hz depending on the location. Each MISP plug also contains an isotherm sensor called Hollow aErothermal Ablation and Temperature (HEAT).[10] The HEAT sensor is designed to measure the temporal progression of 700 ℃ isotherm through the TPS. The sensor elements are conductive, so as the char layer-virgin material interface advances, these elements become shorter and the voltage output decreases. The measurement range for the HEAT sensor is 0 to 13 mm with an accuracy of ± 0.5 mm. The HEAT sensor is sampled at 8 Hz. Figure 2 shows a completed HEAT sensor and MISP plug.

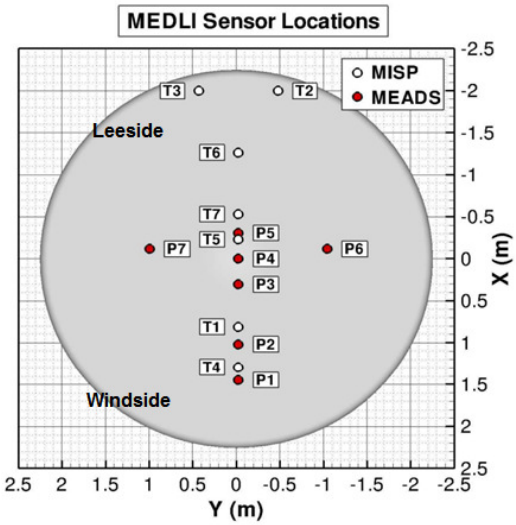

Figure 1. MEDLI sensor locations on the MSL heatshield[4].

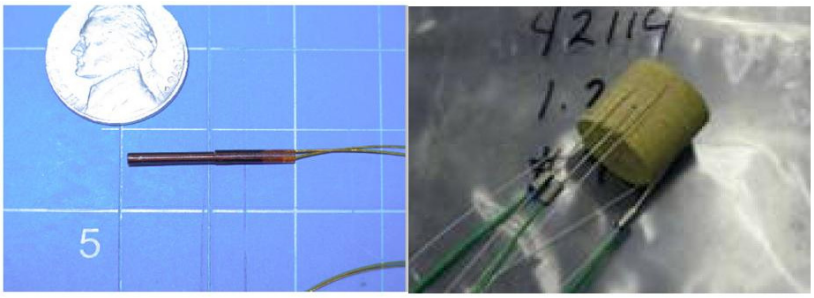

Figure 2. Completed HEAT sensor (left) and MISP plug (right) [10]

III. Methodology

The purpose of this work is to investigate the estimation of MSL surface boundary conditions from simulated MISP temperature data using inverse methods. Typical engineering problems are direct problems where a physical phenomenon is studied using an analytical model. Model parameters and boundary conditions are known and the goal is to compute the system response or model outputs. However, analysis of experimental data is an inverse problem where the measurements of a system's response are available; an analytical model is then used to estimate certain model parameters and/or boundary conditions from the data. Inverse problems are mathematically ill-posed meaning that the conditions of solution existence, uniqueness and stability are not generally satisfied. These problems tend to be unstable and sensitive to random or bias errors. Furthermore, different inputs to the model could result in similar model outputs. Therefore, the estimation of parameters or boundary conditions from measurements of model outputs is not guaranteed to have a unique solution. The non-uniqueness stems from a multi-modal objective function. Regularization techniques are used to redefine the problem such that the new problem is better posed. In the following sections, the estimation problem is defined by selecting the range of boundary conditions to be estimated and the range of simulated data to be used. The inverse methods used in this study are explained, followed by a review of the investigation process and comparison criteria used in the paper.

A. Definition of the Estimation Problem

Similar to all inverse problems, the MSL surface heat flux estimation problem used in this investigation has three parts: direct model, estimation parameters, and simulated data.

1. Direct Model

The current study utilizes the Fully Implicit Ablation and Thermal Response Program (FIAT) with PICA properties to model the TPS material performance and sizing (reference 11). FIAT is an implicit ablation and thermal response program for simulation of one-dimensional transient thermal energy transport in a multilayer stack

of isotropic materials that can ablate from a front surface and decompose in-depth. FIAT has been developed by scientists at the NASA Ames Research Center and is a standard tool in the aerospace industry today for thermal sizing and analysis of spacecraft heatshields. The equations solved in the FIAT code are the internal energy balance, internal decomposition, internal mass balance and surface energy balance equations. The surface energy balance is solved using pre-calculated surface blowing rate, B', tables derived under the assumption of thermochemical equilibrium at the surface. Small modifications were made to FIAT version 2.5 for this work.

2. Estimation Parameters

The purpose of this study is to estimate time-dependent surface heat flux. However, for an ablative material, heat flux is not a direct input to FIAT. Instead, the following surface energy balance equation is solved:

$$C_H\left(H_r-(1+B')h_w\right)+\dot{m}_g h_g+\dot{m}_c h_c+\alpha_w q_{rad}-\sigma\varepsilon_w\left(T_w^4-T_\infty^4\right)-q_{cond}=0 \quad (1)$$

The above equation includes terms representing many of the complex processes that occur at the surface of an ablative material. These terms include the incoming convective heating, the incoming radiation from the shock layer, the reradiation from the TPS material, the material response through pyrolysis and ablation processes and the heat conducted into the TPS material. The recovery enthalpy H_R, surface pressure, radiative heating q_{rad}, blowing correction, and the heat transfer coefficient C_H are inputs to FIAT environment file as a function of time. The B' tables and gas enthalpy are also inputs to FIAT. The boundary layer convective heating is represented by the first term in the above equation. It is not possible to estimate all the terms in the above equation. Therefore, we have to pick the most relevant parameter. In this study, we estimate the heat transfer coefficient C_H which is the main contributor to the incoming convective heating. The other parameters are assumed to be known with low uncertainty. Once the heat transfer coefficient is estimated the resulting heat flux can be calculated using the other parameters. The surface heat flux is the sum of the first three terms in the above equation.

The heat transfer coefficient is a time-dependent parameter. In this study, C_H is discretized every 1 second. This discretization is a balance between the desire to have a higher resolution C_H profile, computational resources and the stability of the inverse methods. Figure 3 shows a plot of the nominal heat flux and heat transfer coefficient for two plug locations, T2 and T4 (highest and lowest heating) for the entire MSL trajectory. These surface conditions were calculated using the Computational Fluid Dynamics (CFD) along DPLR from MSL's nominal design trajectory.[12] This study limits the estimation of the surface conditions for the time range where heat flux is greater than 1 W/cm^2, which corresponds to the time range shown with the black vertical lines (20-150 s).

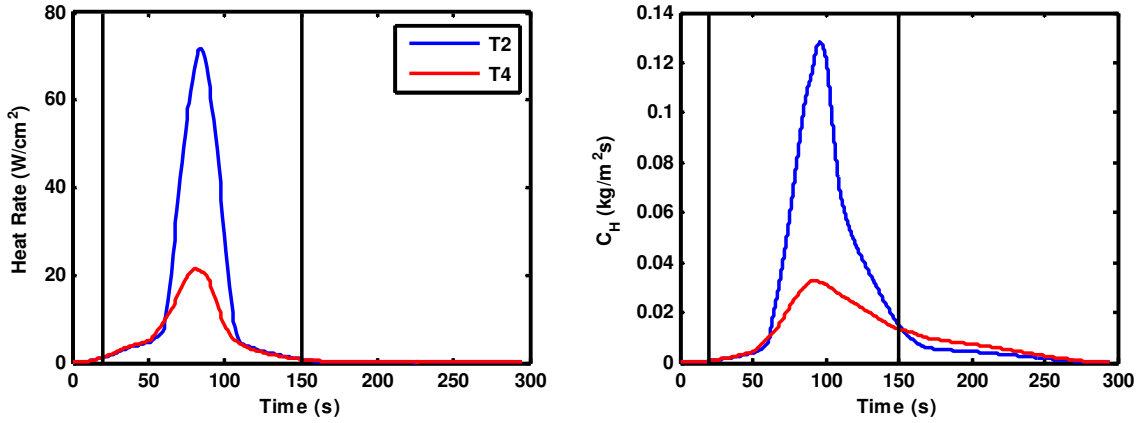

Figure 3. The nominal surface heating conditions for T2 and T4 locations showing the estimation range

3. Simulated Data

As mentioned before, MISP consists of seven plugs at different locations on the heatshield each containing four thermocouples (TC) and an isotherm sensor. In this paper we limit the analysis to the plugs that experience the highest and lowest surface heating, T2 and T4 respectively, to bound the range of surface heating expected by MISP plugs in flight. Currently, the isotherm sensor is going under an extensive testing and calibration program.[13] The purpose of this calibration campaign is to determine the nominal value of the isotherm and the associated uncertainties. The isotherm that this sensor tracks could depend on the temperature change rate as well as the local

temperature. As a result, the current study does not use the isotherm measurements as a part of the data. The heat flux estimation will not greatly benefit from the isotherm data; however, it could be beneficial in determining TPS recession in a future study. The top two TCs are closest to the surface and therefore are most sensitive to the boundary conditions. Furthermore, the actual flight data will carry some bias due to the uncertainty in the material properties. The deeper TCs are affected more by an inaccurate knowledge of material properties. For these reasons, only the top two TCs are used in this work for estimation of surface conditions. For plug T2 the recession front reaches the top TC; therefore, the simulated data for this TC is only used up to the vicinity of the burnout point.

Figure 4a shows a plot of the simulated measurements as a function of time for both plug locations. These measurements were simulated using FIAT and the current nominal heating and material parameters for the MSL vehicle. This plot shows the measurement without any noise/errors. Simulated random and bias noises can be added to the data to study their effect on the estimation results. Random errors are sampled from a normal distribution with a mean of zero and standard deviation of 0.5% of TC temperature, and are added to the simulated data. Figure 4b shows an example of simulated noisy data for the T4 location.

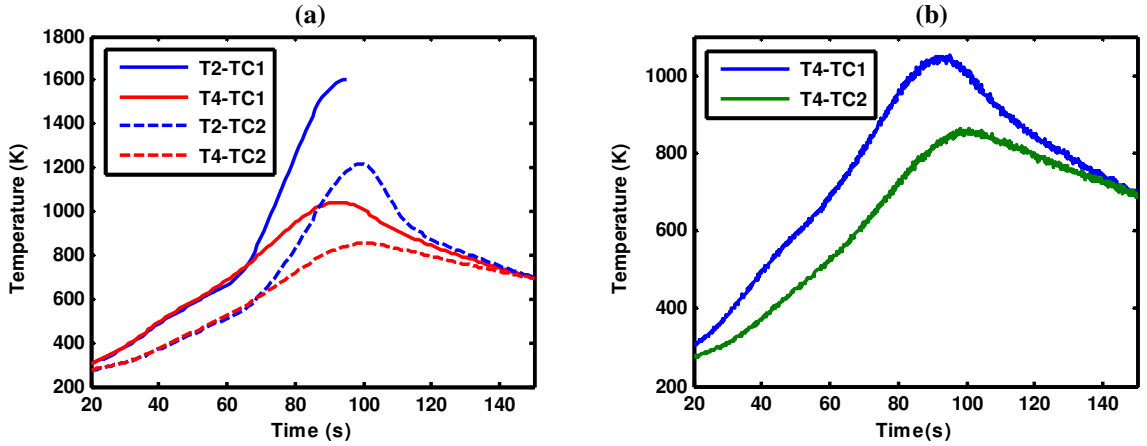

Figure 4. (a) Simulated TC measurements for the two plug locations. (b) T4 simulated data with added random noise

An example of data bias error is TC thermal lag. In this paper, thermal lag is implemented by lagging the simulated TC temperatures using a simple lump capacitance model for an infinitely long wire. At any time step, given the current temperature of the host material (original simulated TC temperature) and the initial wire temperature, the heat transferred from the host material to the wire can calculated for a given contact conductance, h_c, wire properties, volume and surface area. The change in wire temperature for the current time step is then solved using the equation below:

$$\left[\rho C_p V \frac{\Delta T}{\Delta t}\right]_{wire} = h_c A_s \left(T_{host} - T_{wire}\right) \tag{2}$$

For this problem, the properties of a type-K thermocouple are used for the wire properties. Figure 5 shows the lagged TC measurements for different contact conductance values for plug T4. It can be seen that higher contact conductance, h_c results in smaller thermal lag in the TC measurements. In this paper whenever thermal lag is added to the data a nominal contact conductance of 350 W/m^{2}K is used. The effect of varying this parameters on the estimation results are shown later for plug T4.

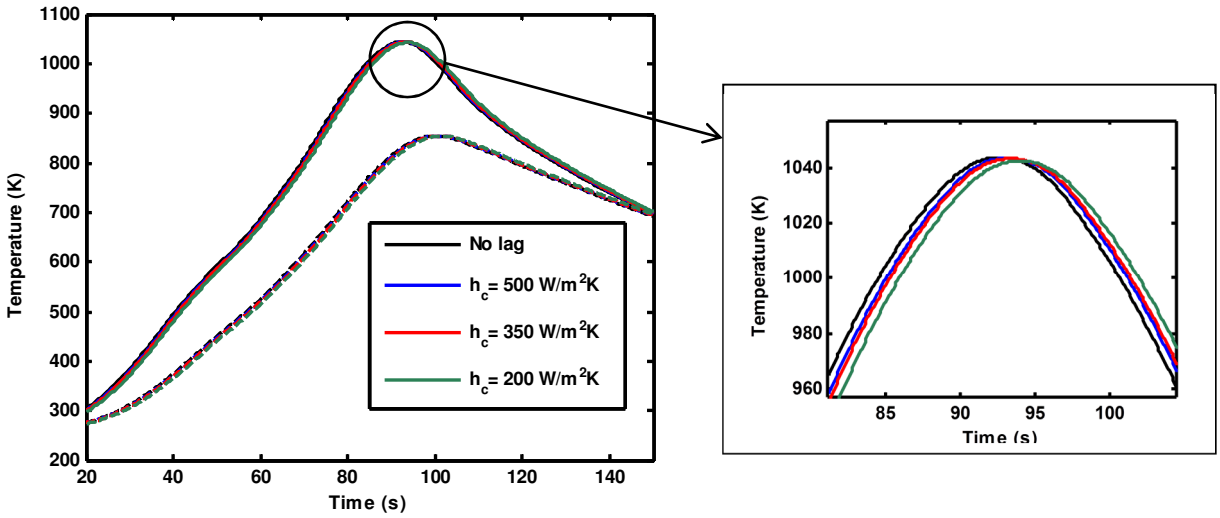

Figure 5. Implementation of TC thermal lag using a simple lump capacitance model for plug T4

B. **Investigation Process**

The TC measurements are simulated using the nominal surface conditions and PICA material response model. The surface C_H profile that generates this data is taken to be the truth or known solution. A simple Gaussian function is used for the initial guess. This represents a realistic starting solution for the actual flight problem because heat rate profiles generally resemble Gaussian functions. As shown in Figure 6, this initial guess looks very different from the known solution and it does not have some of the asymmetry present in the known solution curve. The effect of using a different initial guess is shown later for one of the cases. Figure 6 illustrates the C_H profile used to generate the data and the one used for initial guess for plug T2.

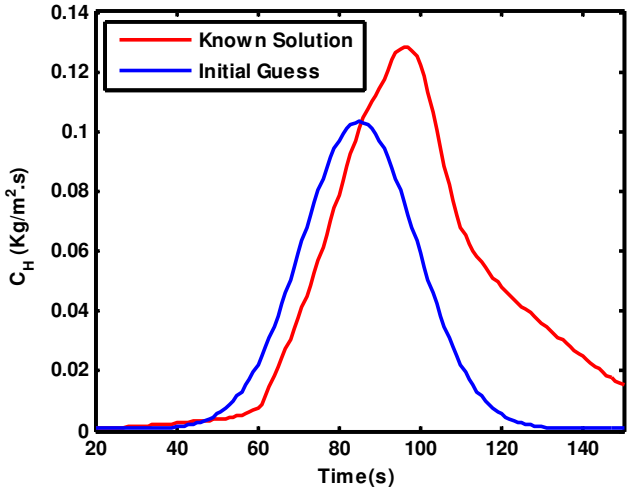

Figure 6. Initial guess compared to the known solution for plug T2

The investigation process begins with the simulation of the TC measurements using the nominal C_H profile and nominal material response model. The simulated data are then used either in this from or with added noise and thermal lag depending on which case is being studied. Once the data is generated, the inverse method starts with the initial guess and attempts to estimate the C_H profile in order to achieve the best match between the TC temperature predictions and simulated data. This is done by iterative minimization of the sum of square of errors between the TC predictions and simulated measurements. This process is continued until convergence is reached and the best-estimate C_H profile is obtained. In addition to random noise and thermal lag, the effect of material property bias on the estimation results is also investigated. This is done by simulating the measurements with a perturbed material response model and then performing the estimation using the nominal model. In this case, we are simulating the situation where our knowledge of material properties is inaccurate, which is expected for flight data. For this study

the material response model is perturbed by increasing either PICA density (all components) by 10% or decreasing thermal conductivity by 10%.

The estimated C_H profiles and the corresponding reconstructed surface heat flux will be compared. In most cases the best-estimate and known solution C_H profiles are co-plotted and compared visually. Another criterion used for comparison is the Normalized Absolute Difference (NAD), which is the absolute difference between the known solution and best-estimate C_H profiles as a percentage of the peak C_H value (shown in equation 3). This criterion is used instead of percent error because a small absolute error when the C_H value is small itself could lead to a large percent error. This criterion can be defined similarly for surface heat flux. Another criterion used for comparison is what is called the Relative Integrated Error (RIE) which is the integrated square of differences between the nominal (known solution) and best-estimate C_H profiles as a percentage of the integrated square of the nominal C_H profile (shown in equation 4). This criterion can be similarly defined for the surface heat flux.

$$Normalized \quad Absolute \quad Difference = 100 \times \frac{\left(C_H^{BE} - C_H^{Nom}\right)}{\max\left(C_H^{Nom}\right)} \tag{3}$$

$$Relative \quad Integrated \quad Error = 100 \times \frac{\int \left(C_H^{BE} - C_H^{Nom}\right)^2 dt}{\int \left(C_H^{Nom}\right)^2 dt} \tag{4}$$

C. Inverse Estimation Methods

Inverse methods have been widely used to solve data analysis problems in a broad range of fields such as heat transfer,[14-18] geophysics,[19] trajectory reconstruction,[20, 21] remote sensing, mathematics, and astronomy. The general methods used in these fields are similar. For that reason and for the sake of brevity, we only focus on the methods used in heat transfer problems. This is not intended to be a complete review of inverse methods, but only the methods relevant to this work.

IHTPs can be categorized in many different ways.[16] They can be classified in accordance with the nature of the dominant heat transfer process: conduction, convection or radiation. Another classification is based on the type of parameters being estimated: boundary conditions,[7] model parameters (material properties),[14] initial conditions or geometric characteristics. This makes the inverse problem either a parameter estimation or function estimation problem. Another classification is based upon the differential equations representing the problem: linear or nonlinear. The temporal and spatial dependence of material properties makes the heat conduction problem nonlinear. The inverse methods used for these problems can also be classified based on the time domain of the measurements used in the estimation process: whole-time domain or sequential. Other ways of classification include the dimension of the heat transfer problem (ex.: 1-D, 2-D or 3-D) and the method of solution of the direct heat transfer problem (ex.: finite difference, finite element, finite control volume, Duhamel's theorem). This inverstigation is concerned with the category of nonlinear Inverse Heat Conduction Problems (IHCP) for the estimation of boundary conditions. The direct problem is solved using FIAT which is a one-dimensional finite difference code.

Two methods that have been considered for this problem are the whole-time domain method and the sequential function specification method. The whole-time domain methods estimate all of the parameters characterizing the boundary condition profile at the same time using all measurements. The estimation is done by iterative minimization of an objective function S (ordinary least square), which is equal to the sum of the square of errors between the measurements and the corresponding temperature predictions. Different methods can be used to perform the minimization such as Gauss-Newton,[14, 17] Levenberg-Marquardt,[16] Box-Kanemasu[14] and different variations of the Conjugate Gradient method.[16] The Gauss-Newton method provides the fastest convergence however it can be unstable. In this paper we use this method and resolve the instability problem with the use of regularization techniques. As explained before inverse problems are ill-posed they become unstable in the presence of errors and for small time steps. This results in large oscillations in the boundary condition estimates. Regularization approaches have to be used in conjunction with the minimization scheme to make the problem better posed and more stable. Regularization has a smoothing effect on the parameter estimates. Russian mathematician Andrey Tikhonov devised a procedure for the regularization of ill-posed problems.[8, 9] His technique involves the addition of a penalty function to the ordinary least square function to alleviate oscillations in the solution. By doing

this, we are effectively solving a neighboring problem that has solution close to the solution of the original problem, with the distinction that the new problem is better posed. The regularization term can take many different forms.

Unlike whole-time domain methods, sequential methods estimate a given parameter using only a limited range of measurements and continue sequentially in time. One of the leading methods is the function specification method with future time algorithm developed by James Beck.[7] In this method the boundary condition at a given time is estimated using TC measurements for only a limited future time window. Then the solutions are saved and the method continues to the next time step. The number of future time steps used in the estimation has the same effect as the regularization approach used for the whole-time domain methods. This method has the advantage of being more computationally efficient than whole-time domain methods, but less stable. However, to benefit from this efficiency, the code used to solve the direct problem must be able to save and restart the solution in time. FIAT does not currently offer this option. For this reason and the higher stability of whole-time domain methods, they are used for this study. The authors are currently working with NASA Ames Research Center personnel to modify FIAT to allow a restart option, and will perform similar analyses with the future time function specification method once this option becomes available.

1. Gauss-Newton Algorithm

The Gauss-Newton algorithm is widely used to solve nonlinear least squares problems.[14, 16] It is a modification of Newton's method which does not require the knowledge of second derivatives. The algorithm iteratively minimizes the ordinary least square objective function S, which is equal to the sum of square of differences between measurements and temperature predictions shown below in matrix form at iteration *k*:

$$S\left(\mathbf{P}^k\right)=\left[\mathbf{Y}-\mathbf{T}\left(\mathbf{P}^k\right)\right]^T\left[\mathbf{Y}-\mathbf{T}\left(\mathbf{P}^k\right)\right] \tag{5}$$

where P is the vector of parameters being estimated (discretized C_H values), Y is the vector of the simulated TC measurements (TC1 and 2 combined) and T is the corresponding vector of temperature predictions. The Gauss-Newton method is developed by deriving the gradient of the above equation, linearizing the vector of predicted temperatures T(P) with a Taylor series expansion around the current solution P^k and setting the gradient of S to zero. The expression can be rewritten to derive the change in parameters ΔP required to minimize S:

$$\mathbf{J}^{k\,T}\mathbf{J}^k\,\Delta\mathbf{P}^k=\mathbf{J}^{k\,T}\left[\mathbf{Y}-\mathbf{T}\left(\mathbf{P}^k\right)\right] \tag{6}$$

where J is the Jacobian matrix which is equal to the derivative of the predicted TC temperatures to estimation parameters (discretized points along the C_H profile) as shown in the equation below:

$$\mathbf{J}=\begin{bmatrix}\dfrac{\partial T_1}{\partial P_1} & \cdots & \dfrac{\partial T_1}{\partial P_N}\\ \vdots & & \vdots\\ \dfrac{\partial T_M}{\partial P_1} & \cdots & \dfrac{\partial T_M}{\partial P_N}\end{bmatrix} \tag{7}$$

where *M* is number of measurement and *N* is the number of estimation parameters. The calculation of this Jacobian matrix is where most of the inverse problems difficulties arise and is computationally expensive because its numerical approximation requires *N* solutions of the direct problem. This procedure is continued until a stopping criterion is reached. A range of convergence criteria can be used for this problem. Iteration can be stopped when S reaches a small number or when the percent or absolute change in S is small. Another criterion could be to stop the iteration once the absolute or percent change in estimation parameters is smaller than a specified value. A maximum number of iteration is another criterion. These criteria are all implemented in the inverse code; however, in the presence of errors they might never be satisfied because the objective function cannot be reduced to small numbers. An approach widely used in literature is the discrepancy principle in which the iteration is stopped once S reaches the expected error in the data.[15] This would be equal to $M\sigma^2$ where σ is the standard deviation of the measurement errors. This approach is useful when the errors are known and normal and have a constant standard deviation. However, in reality this assumption is not always valid. Furthermore, if measurements have bias errors this approach cannot be used. Therefore, in order to develop methods that can be similarly applied to the case of flight data, this criterion is not used in this work. The iterations are continued for a specified maximum number and the best

estimate is taken to be when the solution is stable. In this work, the maximum number of iterations was set to 200 to make sure that a converged solution is reached.

2. Tikhonov Regularization

Tikhonov technique is used to regularize the ill-posed inverse problem and alleviate the non-physical oscillations that occur in the boundary condition estimate.[7, 8] First order Tikhonov regularization has proved to be the most effective for the surface heating estimation problems and is therefore used here. The penalty function added is the sum of square of differences between the consecutive C_H values. Equations 5 and 6 need to be modified accordingly:

$$S = [\mathbf{Y} - \mathbf{T}]^T [\mathbf{Y} - \mathbf{T}] + \mu [\mathbf{H1} \times \mathbf{P}]^T [\mathbf{H1} \times \mathbf{P}] = \sum_{i=1}^{M} (Y_i - T_i)^2 + \mu \sum_{j=1}^{N-1} (P_{j+1} - P_j)^2 \tag{8}$$

$$\left[\mathbf{J}^T \mathbf{J} + \mu \mathbf{H1}^{\mathrm{T}} \mathbf{H1}\right] \Delta \mathbf{P} = \mathbf{J}^T [\mathbf{Y} - \mathbf{T}] \tag{9}$$

$$\mathbf{H1} = \begin{bmatrix} -1 & 1 & 0 & \cdots & 0 \\ 0 & -1 & 1 & \cdots & 0 \\ \vdots & \ddots & \ddots & \ddots & \vdots \\ 0 & \cdots & 0 & -1 & 1 \\ 0 & 0 & \cdots & 0 & 0 \end{bmatrix} \tag{10}$$

Small values of μ ensure rapid minimization of the ordinary least square function, but result in large oscillations in the C_H profile. Larger values of μ reduce oscillations, but slow down the minimization of the objective function. There are different methods and criteria in the literature for the selection of this parameter. The general approach used here is to start with a small value of μ and increase it until the obtained estimate is satisfactory and the degree of oscillations is reduced sufficiently. Qualitatively a good solution is a solution that traces through the unregularized oscillatory solution. The μ values that worked for this problem ranged from 10^9 to 10^{12}. This might seem too large compared to the values seen in literature, but it should be noted that most of the work in literature involves the estimation heat flux which is orders of magnitude greater than C_H. In the case of simulated data with no noise, regularization was not needed and an almost perfect estimate was obtained using the Gauss-Newton method.

IV. Implementation & Results

This section provides the estimation results for the different noise cases for both plug locations. Furthermore, brief discussions on the effects of the initial guess, regularization parameter, and contact conductance are presented. Figure 7 shows the estimation results for the simulated data without any noise. Only normalized absolute difference is shown here because the best estimate profile is almost the same as the known solution. We can clearly see that the C_H profile is estimated very well and the normalized absolute difference is very close to zero for the entire profile. In the same figure, similar results are obtained for plug T4. The errors are in the order 10^{-5} %.

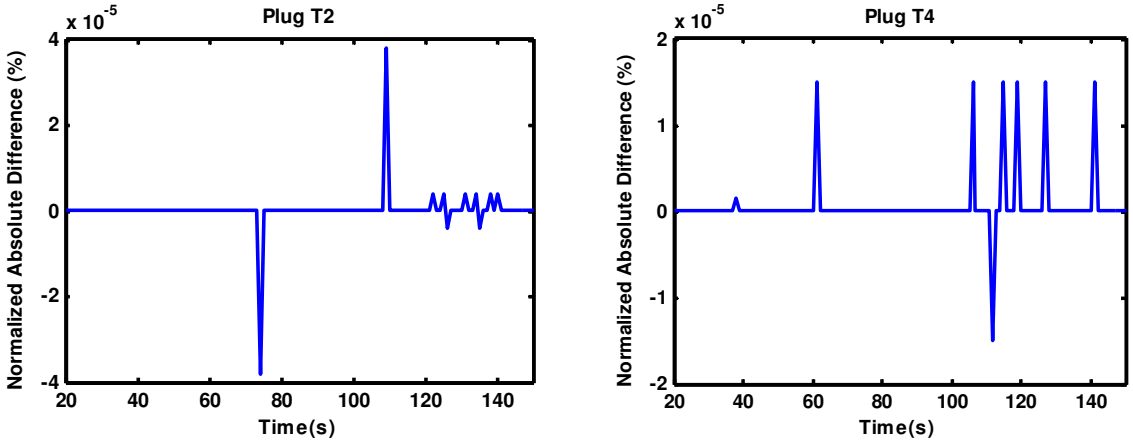

Figure 7. Error in the best estimate C_H profile for the case of simulated data without noise

These results are obtained with the Gaussian initial guess. In order to study the effect of the initial guess on the estimated profile, the estimation is also repeated for a constant C_H initial guess (10% of the peak C_H value) for the T2 location. Figure 8 compares the estimation results and convergence behavior for these two initial guesses. The original initial guess is labeled as "IG 1" while the constant 10% initial guess is labeled as "IG 2". We can clearly see that in both cases the estimated profile is very close to the known solution and very similar estimates are obtained. However, as expected, a more difficult initial guess takes longer to converge. We can see in the right plot that the simple initial guess case takes 7 iterations to converge while the constant initial guess case takes 24 iterations.

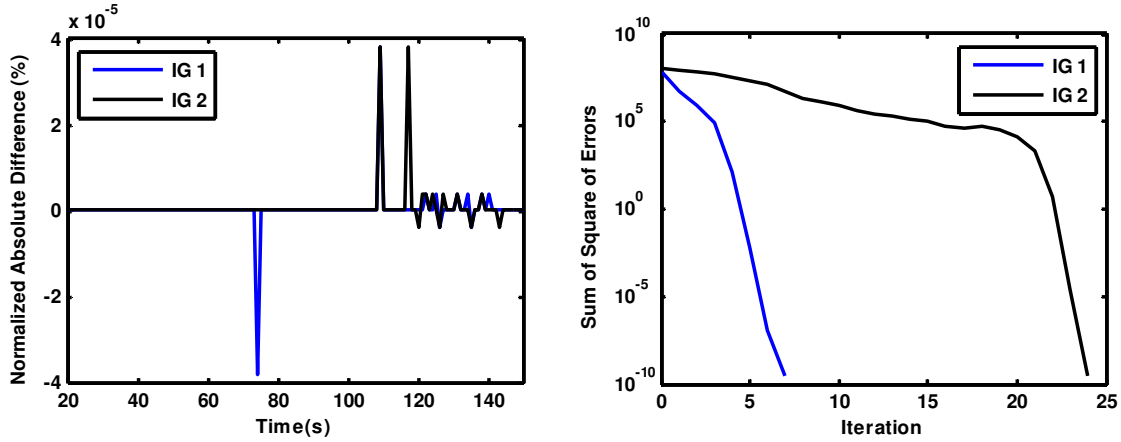

Figure 8. The effect of initial guess on the estimation results and convergence behavior

Figure 9 shows the estimation result for the case of simulated data with random noise for both plug locations. We can clearly see that without regularization the solution is oscillatory.

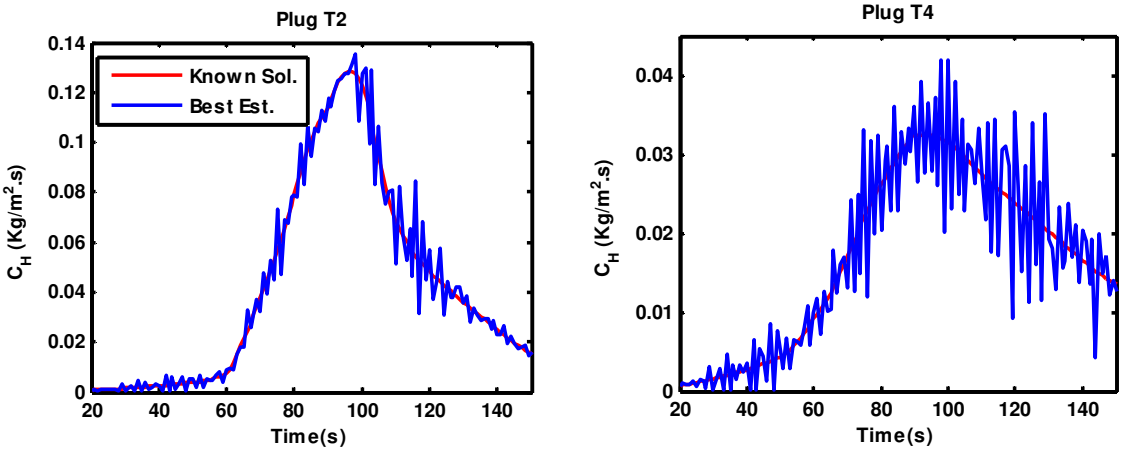

Figure 9. Estimation in the case of simulated data with random noise with no regularization

Figure 10 and Figure 11 show the results for the same estimation performed with Tikhonov first order regularization. The oscillations have been substantially reduced and the best-estimate C_H profile is very close to the known solution. The right plot in Figure 10 shows the residuals between best estimate temperature predictions and the measurements. As expected we can see that the difference in temperatures after estimation is random around zero, and with similar distribution as the added random noise to the data. Figure 11 illustrates the normalized absolute difference between the best-estimate and known solution C_H profiles for both plug locations. We can see that even in the presence of relatively substantial random noise the estimation results are very good and within 1% of the peak value.

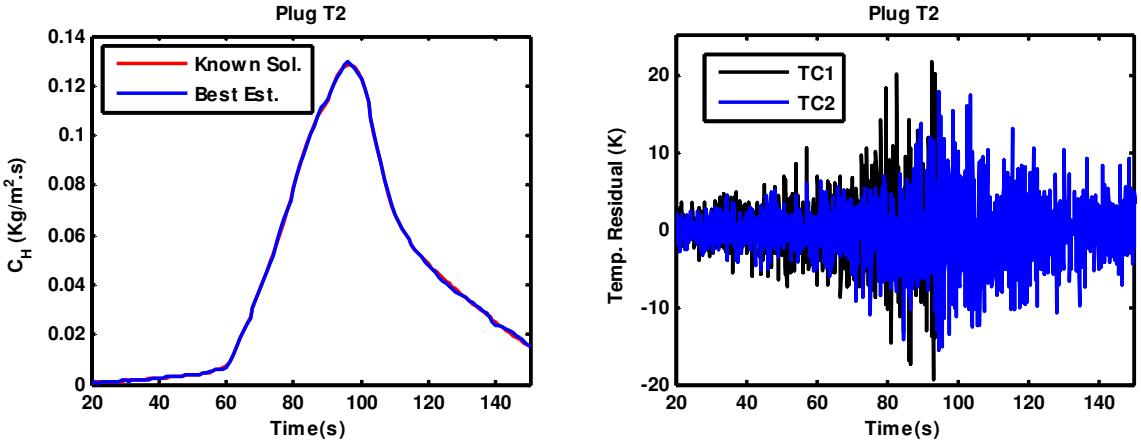

Figure 10. The case of simulated data with random noise with regularization for T2

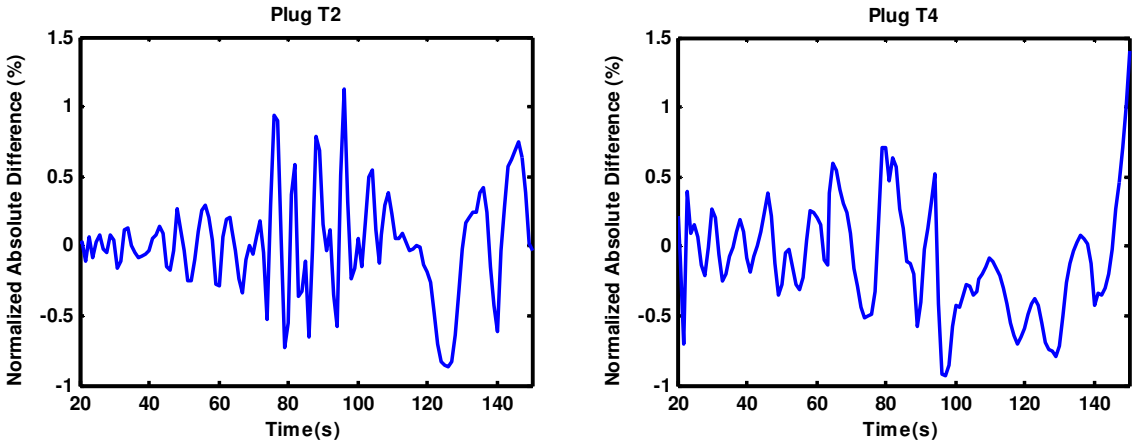

Figure 11. Estimation errors in the case of data with random noise with regularization

In Figure 12, the effect of regularization parameter on the estimated profile for plug T2 is presented. The estimation is performed for two values: 10^9 and 10^{11}.

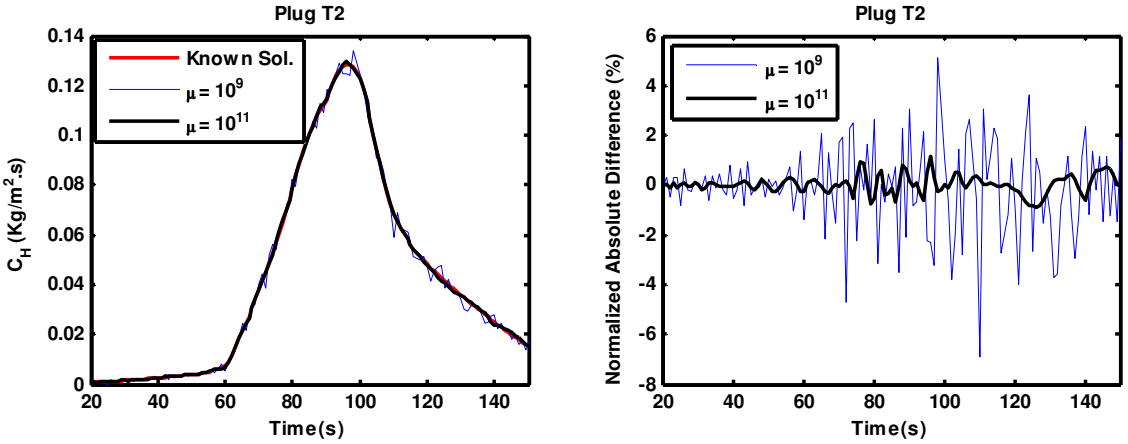

Figure 12. The effect of regularization parameter on the estimation results

It can be observed that the estimate for the higher regularization parameter is better and less oscillatory. Comparing these results with the unregularized estimate (μ=0) shown in Figure 9, it is clear that increasing μ will greatly reduce the oscillations in the solution. However, it should be noted that there is a diminishing return where

high values of μ over-penalize the solution and substantially slow down the reduction of the objective function and solution convergence. Therefore, a good strategy for the selection of the regularization parameter is to increase it until the oscillations in the final estimate have been reduced enough and the estimate still traces the general trend of the unregularized estimate closely. The results for the remaining cases are shown only for the regularized estimates, but the same trend is seen

Figure 13 demonstrates the estimation results for the case of simulated data with thermal lag for both plugs. The simulated data are lagged with a thermal conductance of 350 W/m^2 K. Thermal lag in the data is a bias error and we can see that there is a bias error in the estimated C_H profile. The estimated profile lags the original C_H curve the same way the simulated TC measurements lag the original TC measurements. The lag is more pronounced on the decreasing half of the C_H curve due to the fact that the effective heat rate is lower compared to the increasing side (see Figure 3).

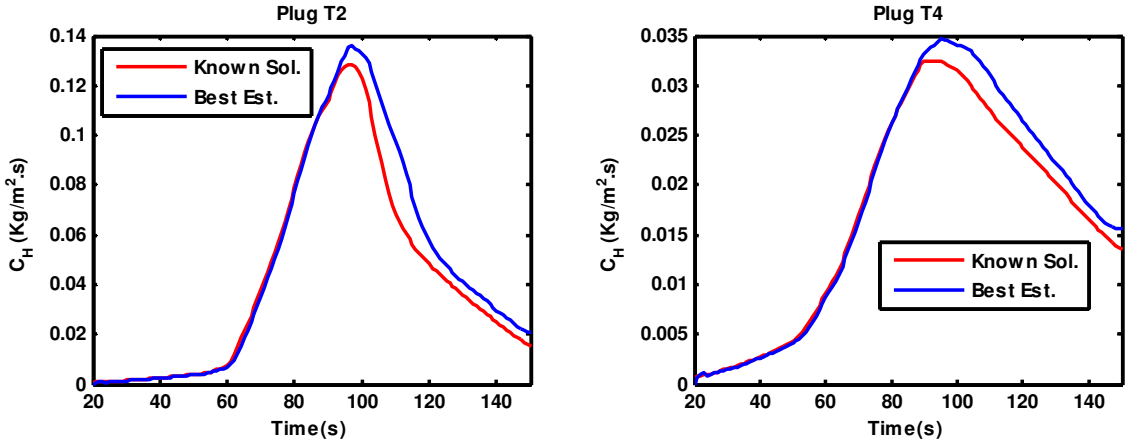

Figure 13. Estimation results in the case of data with thermal lag

In Figure 14, the estimation is performed for the simulated data with thermal lag for plug T4 for three different values of contact conductance. This is done to show the effect of the magnitude of thermal lag on the estimated C_H profile.

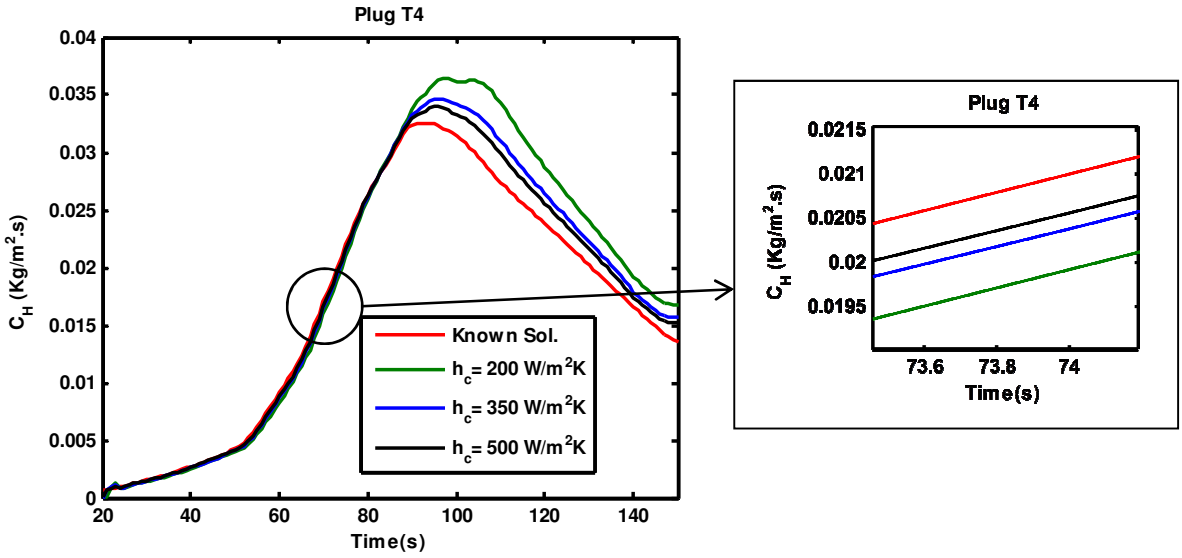

Figure 14. The effect of contact conductance in lag modeling on estimation results

We observed that the thermal lag in the simulated data increases with a lower contact conductance (Figure 5). As expected the higher lag in the subsurface thermocouple data results in a larger bias error in the estimated surface C_H profiles. We can see that the estimated profile lags the original one in the same way that the lagged data lags the

original simulated data. Estimated C_H is initially lower than original C_H and then it crosses over and exceeds the original curve after about 80 s. The results from Figure 13 and Figure 14 confirm that a large thermal lag in the TC data could result in a large error in the estimated profile. Therefore, in the case of the analysis of flight data, it is best to model TC lag as accurately as possible and either implement this effect within FIAT or correct the data.

Figure 15 demonstrates the effect of the PICA density perturbation on estimation results for both plugs. In this case, the data is simulated using a perturbed PICA thermal response model with 10% higher density (all components for virgin and char) and then the original response model (lower density) is used in the estimation of C_H curve. C_H and material density have similar but opposite effects on the in-depth material temperature response. Generally, higher surface C_H results in higher subsurface temperatures while higher material density results in lower subsurface temperatures. Therefore, if a lower density material model is used in the estimation process compared to the one used to generate the data, the predicted subsurface temperatures will be higher, and the estimated C_H will be lower to compensate for the higher subsurface temperatures. This is exactly what is seen in the estimation results. This shows that the strong linear dependency between C_H and material density results in a direct translation of the bias error in material density to a bias error in estimated C_H profile.

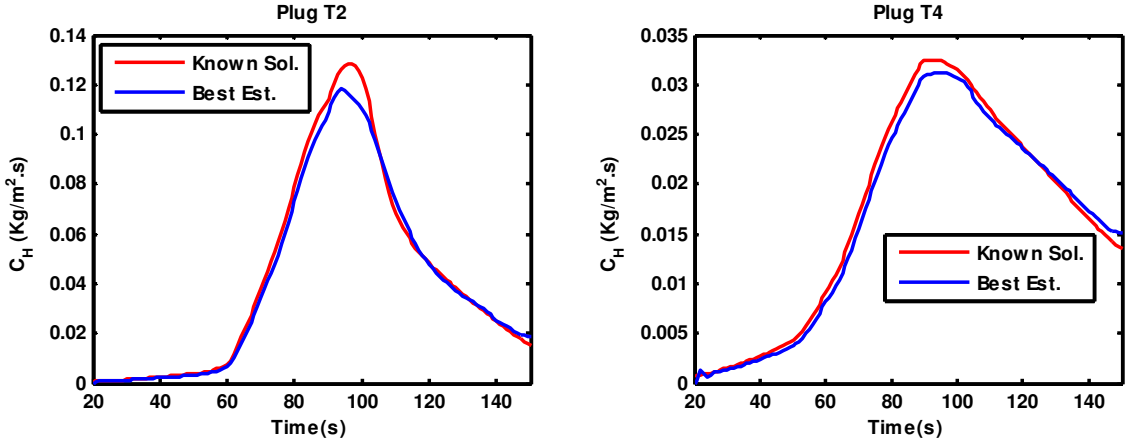

Figure 15. Estimation results in the case of data with PICA density perturbation

Figure 16 shows the effect of the PICA thermal conductivity perturbation on the estimation results for both plugs. The simulated data are generated with a material model with 10% lower conductivity (virgin and char) and then the original material model (higher conductivity) is used in the estimation process.

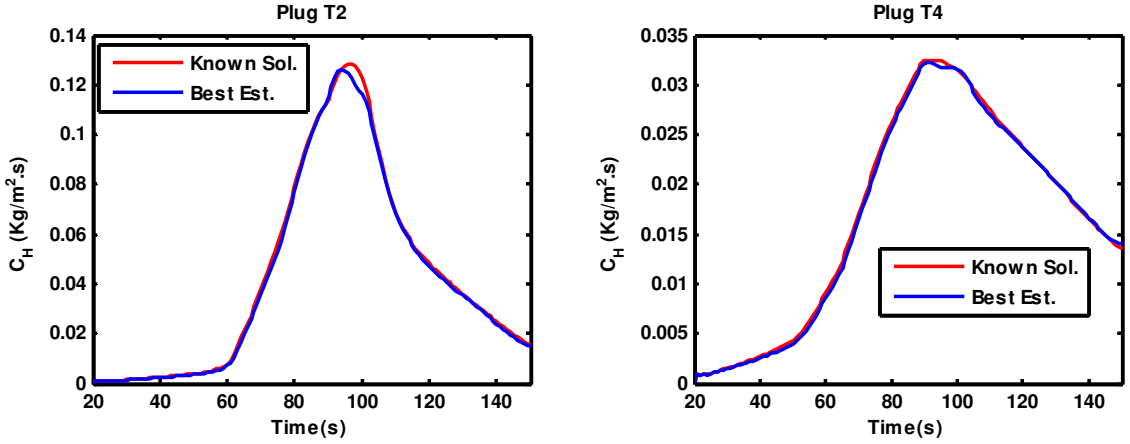

Figure 16. Estimation results in the case of data with PICA conductivity perturbation

Higher conductivity results in higher predicted subsurface temperatures and we expect a bias error in the estimated C_H profile. However, C_H and thermal conductivity are not as linearly dependent as C_H and density, therefore, even though there is a bias error in the estimated profile it is not as large as the density perturbation case.

In other words, due to the lower linear dependency between C_H and conductivity, a large reduction in C_H profile does not completely compensate for the bias error in the data, and the estimated profile is closer to the original curve.

Figure 17 and Figure 18 show the estimation results for both plugs for the simulated data with random noise, thermal lag (h_c = 350 W/m^2 K) and material property bias (density perturbation). The estimated C_H profile shows a combination of both lag and material property biases seen before. These errors result in a C_H profile that is not the same as the profile used to generate the data. Such errors and biases in the measurements and models are expected within the flight data. Therefore, it is very crucial to correct for these errors and biases in order to ensure an accurate estimation of surface boundary conditions.

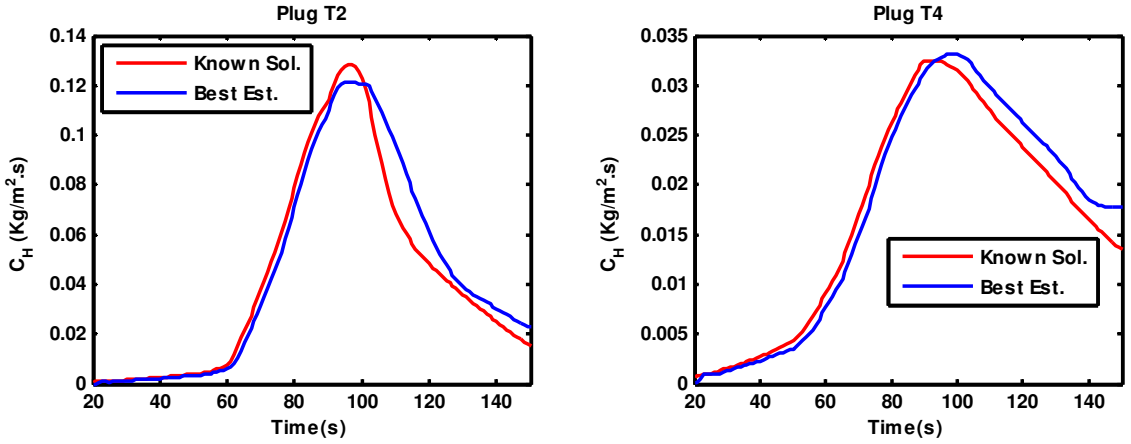

Figure 17. Estimated C_H profile in the case of data with combined errors

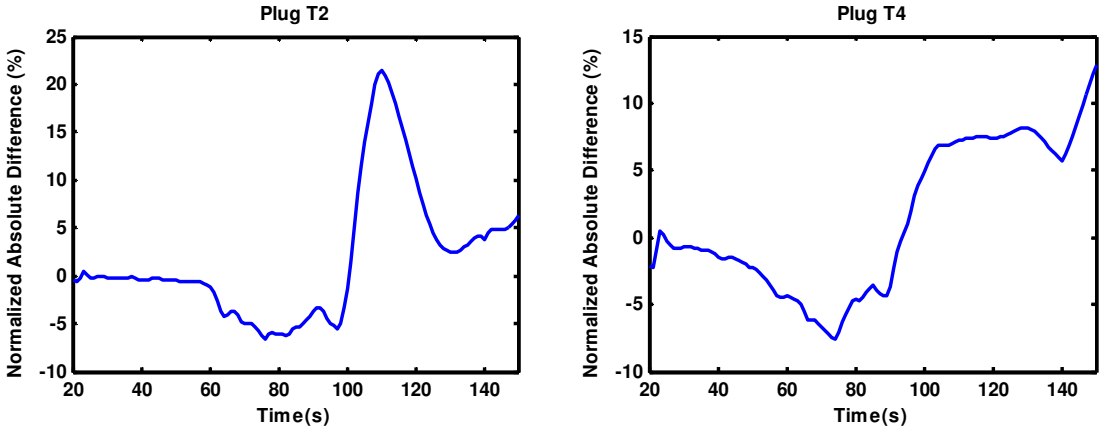

Figure 18. Estimated C_H normalized absolute difference in the case of data with combined errors

As mentioned before, the surface heat transfer coefficient is the parameter that is estimated in this study because the surface heat flux is not a direct input for ablation modeling in FIAT. All the results above were shown for the reconstructed C_H profile. However, once the surface C_H is estimated the heat flux can be calculated by adding the surface convective heating term and the chemical heating term from FIAT outputs (as shown in equation 1). The reconstruction of the surface heat flux is of the primary concern for the MEDLI post-flight analysis and the reconstruction accuracy requirements are stated for heat flux not C_H. Therefore, in this study, the final accuracy criteria will be given for the surface heat flux. Figure 19 shows the reconstructed surface heat flux for the case with combined errors for both plugs (corresponding to C_H estimation in Figure 17). The difference between the known solution and best estimate profiles look somewhat different from the trends observed for C_H profiles. From Figure 20, we can clearly see that the errors in heat flux profile are smaller than C_H profile.

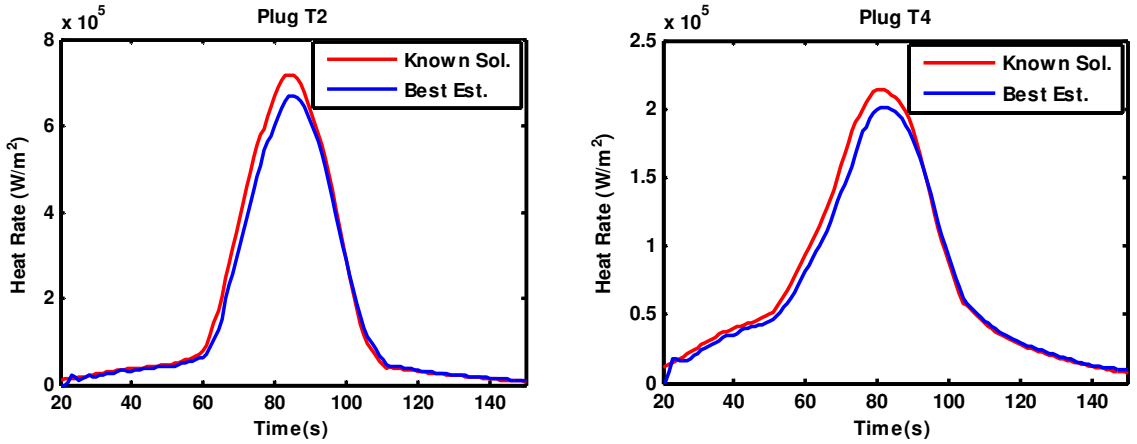

Figure 19. Estimated surface heat flux for the case of combined errors

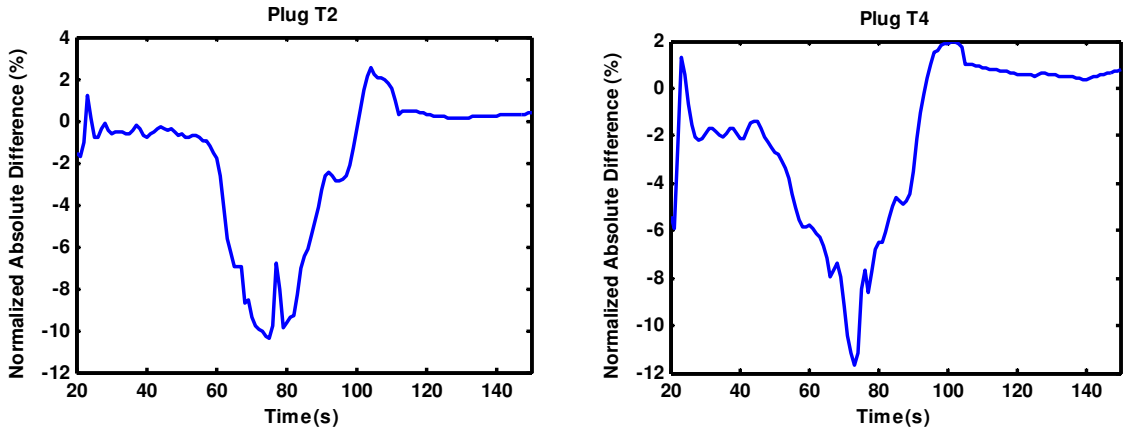

Figure 20. Estimated surface heat flux normalized absolute difference for the case of combined errors

Table 1 provides a summary of the accuracy of the heat flux estimation results for the different cases that are investigated in this paper. These accuracy criteria are calculated and shown for estimation of both plugs for the six cases studied: no error, random noise, TC thermal lag, density perturbation, conductivity perturbation and the combined error cases. In addition to the observations made for each case, we can see that the estimation results for T2 are generally less accurate than T4. This is expected due to the fact that the top TC burns around 95s for T2 and only TC2 data is available for the rest of the period. TC2 is deeper and consequently less sensitive to the surface conditions and more prone to uncertainties compared to TC1. Therefore, the estimation results are less accurate when the top TC data is not available completely.

Table 1. Accuracy of surface heat rate estimation in the presence of different types of errors

	Plug T2		***Plug T4***	
	NAD range (%)	RIE (%)	NAD range (%)	RIE (%)
No Noise	[-6 e-5, 1 e-5]	2.0 e-12	[-1 e-5, 5 e-5]	2.0 e-13
Random Noise	[-1.2, 1.5]	0.0070	[-0.7, 1.0]	0.0061
Thermal lag	[-4.0, 3.0]	0.1727	[-3.5, 3.5]	0.1143
ρ perturbation	[-7.5, 0.5]	0.5230	[-8.0, 0.5]	0.4986
κ perturbation	[-5.0, 1.2]	0.1076	[-3.5, 0.5]	0.0909
Combined Errors	[-10.5, 2.5]	0.9151	[-11.0, 2.0]	0.6084

V. Conclusions

In this paper, the estimation of MSL surface heat transfer coefficient from simulated subsurface temperature data was investigated. Whole-time domain Gauss-Newton least square minimization method in conjunction with Tikhonov first-order regularization was used to perform the estimation. The performance of the inverse methods and the accuracy of the estimated boundary conditions were investigated in the presence of different measurement errors such as random noise, TC thermal lag and model bias errors such as TPS material density and thermal conductivity perturbation. Due to the fact that the data were simulated and the true solution was known, this study was able to inform the level of accuracy with which the surface conditions can be reconstructed from subsurface temperature measurements using inverse techniques.

We observed that regularization is crucial in reducing the oscillations in the estimated C_H profiles. Regularization was required in order to obtain a smooth estimate in all cases except the case without any errors. A good estimate was obtained in the case of data with random noise. However, bias errors in the data such as TC thermal lag resulted in a large bias in the estimated boundary conditions. This proves the necessity of implementing accurate lag models in FIAT or the correction of TC data for thermal lag. A simple capacitance model was used in this study to simulate TC lag; nevertheless, this analysis can be repeated once more accurate Finite Element Analysis (FEA) lag modeling or experimental data is available for thermal lag in MISP plugs. Bias error in the model, such as PICA density or conductivity perturbations, resulted in a bias in the estimated surface C_H profile. Such bias is larger in the case of density perturbations compared to conductivity perturbations. This is due to the stronger linear dependency between C_H and material density.

This investigation focused on the estimation of surface heating boundary conditions from simulated MEDLI data. However, a bias error in the thermal response model such as inaccurate knowledge of material properties was shown to produce an inaccurate estimation of surface conditions. This motivates the use of a comprehensive methodology to target the estimation of material properties in addition to surface conditions. A TC driver approach will be used for the estimation of both surface heating and material response from MISP flight data. In this approach, problem is decoupled by using the data from the top TC as the boundary condition and calculating the simpler heat conduction problem for the TPS block below that TC. This way we temporarily eliminate the surface boundary conditions and their effect on the material response below the top TC. Now the developed IPE methodology for multi-parameter estimation can be applied to the TC driver problem to estimate material properties from the remaining deeper TC data. Once the material properties are updated with this new estimate, we can solve the normal ablation problem and use the top TCs to estimate the time-dependent surface conditions as detailed in this paper.

Acknowledgments

This work was funded by the NASA grant NNX12AF94A from the NRA Research Opportunities in Aeronautics 2010. The authors are grateful to Todd White for providing MISP CFD environments used in this analysis and his help with some modifications made to FIAT. We are also grateful to Brandon Oliver and Adam Amar for their help with TC thermal lag modeling. We would like to thank Ioana Cozmuta, Deepak Bose, Jose Santos, Bernie Laub, Michael Wright, Y.-K. Chen, Soumyo Dutta, and David Hash for their guidance and time to discuss some aspects of this work.

References

[1] Wright, M., Chun, T., Edquist, K., Hollis, B., Krasa, P., and Campbell, C., "A Review of Aerothermal Modeling for Mars Entry Missions," *48th AIAA Aerospace Sciences Meeting*, AIAA 2010-44, January 2010.

[2] Wright, M.J., Milos, F.S., and Tran, P., "Afterbody Aeroheating Flight Data for Planetary Probe Thermal Protection System Design," *Journal of Spacecraft and Rockets*, Vol. 43, No. 5, 2006, pp. 929-943.

[3] Milos, F., Chen, Y.-K., Congdon, W., and Thornton, J., "Mars Pathfinder Entry Temperature Data, Aerothermal Heating, and Heatshield Material Response," *Journal of Spacecraft and Rockets*, Vol. 36, No. 3, 1999, pp. 380– 391.

[4] Edquist, K.T., Dyakonov, A.A., Wright, M.J., and Tang, C.Y., "Aerothermodynamic Design of the Mars Science Laboratory Heatshield," *41st AIAA Thermophysics Conference*, AIAA 2009-4075, June 2009.

[5] Gazarik, M., Wright, M., Little, A., Cheatwood, F. M., Herath, J., Munk, M., Novak, F., and Martinez, E., "Overview of the MEDLI Project," *IEEE Aerospace Conference*, IEEE 2008-1510, Big Sky, Montana, March 2008.

[6] Mahzari, M., Cozmuta, I., Clark, I., Braun, R., "An Inverse Parameter Estimation Methodology for the Analysis of Aeroheating and Thermal Protection System Experimental Data," *42nd AIAA Thermophysics Conference*, AIAA 2011-4027, Honolulu, Hawaii, June 27-30, 2011.

[7] Beck, J.V., Blackwell, B., and St. Clair, C.R., *Inverse Heat Conduction, Ill-posed Problems*, Wiley, New York, 1985.
[8] Tikhonov, A. N., and Arsenin, V. Y., *Solution of Ill-Posed Problems*, Winston & Sons, Washington, DC, 1977.
[9] Tikhonov, A. N., Leonov, A. S, and Yagola, A. G., *Nonlinear Ill-posed Problems*, Chapman & Hall, London, 1998.
[10] Oishi, T., Martinez, E., Santos, J., "Development and Application of a TPS Ablation Sensor for Flight," *46th AIAA Aerospace Sciences Meeting*, AIAA Paper 2008-1219, January 2008.
[11] Chen, Y.K., and Milos, F.S., "Ablation and Thermal Response Program for Spacecraft Heatshield Analysis", *Journal of Spacecraft and Rockets*, Vol. 36, No. 3, 1999, pp. 475-483.
[12] Cozmuta, I., White, T., Santos, J., Laub, B., Mahzari, M., "Proposed Analysis Process for Mars Science Laboratory Heat Shield Sensor Plug Flight Data," *42nd AIAA Thermophysics Conference*, AIAA 2011-3957, Honolulu, Hawaii, June 27-30, 2011.
[13] Santos, J., Jacobs, T., Martinez, E., "Isotherm Sensor Calibration Program for Mars Science Laboratory Heat Shield Flight Data Analysis," *42nd AIAA Thermophysics Conference*, AIAA 2011-3955, Honolulu, Hawaii, June 27-30, 2011.
[14] Beck, J.V., and Arnold, K. J., *Parameter Estimation in Engineering and Science, Wiley, New York, 1977.*
[15] Alifanov, O. M., *Inverse Heat Transfer Problems*, Springer-Verlag, New York, 1994.
[16] Özisik, M. N., and Orlande, H. R. B., *Inverse Heat Transfer: Fundamentals and Applications,* Taylor and Francis, New York, 2000.
[17] Woodbury, K. A., *Inverse Engineering Handbook*, CRC Press, Boca Raton, 2003.
[18] Kurpisz, K. and Nowak, A. J., *Inverse Thermal Problems*, WIT Press, Southampton, UK, 1995.
[19] Aster, R., Borchers, B., and Thurber, C., *Parameter Estimation and Inverse Problems,* Elsevier Academic Press, Burlington, 2005.
[20] Dutta, S., and Braun, R.D., "Mars Entry, Descent, and Landing Trajectory and Atmosphere Reconstruction," *48th AIAA Aerospace Sciences Meeting*, AIAA Paper 2010-1210, Orlando, FL, January 2010.
[21] Dutta, S., Braun, R.D., Russell, R.P., Clark, I.G., and Striepe, S.A., "Comparison of Statistical Estimation Techniques for Mars Entry, Descent, and Landing Reconstruction from MEDLI-like Data Sources," *50th AIAA Aerospace Sciences Meeting*, AIAA 2012-0400, Nashville, TN, January 2012.